

ELECTROCHEMICAL AND SURFACE STUDY OF THE OXIDE GROWTH AND CONVERSION ON 316L STAINLESS STEEL

Quintin W. Knapp and Jungsook Clara Wren

Western University
London, Ontario, Canada, N6A 5B7
qknapp@uwo.ca

Summary

Oxide formation and conversion mechanism as a function of potential on 316L stainless steel was investigated using electrochemical and surface analysis techniques. All of the results were consistent with the electrochemical thermodynamics. Four potential regions were identified for anodic oxidation. In Ox I, conversion of the defective chromium oxide layer to an iron/chromium spinel phase occurred. This was followed by conversion of the upper Fe₃O₄ oxide to a passivating γ -Fe₂O₃ layer in Ox II. At potentials > 0.0 V_{SCE}, Ox III and IV involved the formation of γ -FeOOH and conversion of Cr^{III} to soluble Cr^{VI} respectively contributing to film breakdown.

1. Introduction

Stainless Steel is a material used in nuclear reactors. For such material applications, corrosion must be evaluated in the presence of ionizing radiation. The high radiation fields present in a reactor core will cause water to decompose to a range of highly oxidizing (e.g., •OH, H₂O₂) and reducing (e.g., •e_{aq}⁻, •O₂⁻) species [1]. These redox active species will affect the electrochemical potential of the coolant water phase and hence, the potential on the corroding surface (i.e. the corrosion potential, E_{CORR}). For example, γ -irradiation (at a dose rate of 5.7 kGy·h⁻¹) increases the steady-state E_{CORR} on 316L SS from -0.4±0.05 V_{SCE} to 0.05±0.05 V_{SCE} [2].

The overall objective of the current study was thus to establish the mechanism of the oxide formation and conversion as a function of corrosion potential (or electrode potential) covering the range of potentials that may be reached under irradiation conditions. The oxide formation was studied under both potentiodynamic and potentiostatic conditions and surface analysis techniques (ex-situ X-ray photoelectron spectroscopy).

2. Experimental

All electrochemistry was performed in a three-electrode electrochemical cell consisting of a 316L stainless steel working electrode (WE), a Pt mesh counter electrode, and a saturated calomel reference electrode. Prior to each experiment, the WE was manually polished to a mirror finish, rinsed with distilled water and sonicated in an acetone/methanol (1:1) mixture for 5 min.

Experiments were conducted at room temperature in Ar purged 0.01 mol dm⁻³ borate buffer solutions adjusted to pH 10.6 with NaOH. Prior to the start of all electrochemical experiments, the WE was cathodically cleaned potentiostatically (-1.1 V_{SCE} for 5 min). Cyclic voltammetry (CV) experiments were performed as a function of upper potential limit, pH, potential scan rate and electrode rotation rate. CVs had a scan rate of 5 mV·s⁻¹ unless otherwise noted. Potentiostatic polarization experiments were made as a function of time while periodically recording EIS (not reported below). After potentiostatic measurements, SS electrodes were further analysed by XPS.

3. Results and Discussion

3.1 Oxide Formation and Conversion under Potentiodynamic Conditions

Cyclic voltammetry was performed to establish characteristic potential ranges for the oxide formed on SS at pH 10.6 under potentiodynamic conditions. Assignment of the cyclic voltammograms current peaks was aided by the thermodynamic equilibrium potentials of the redox reactions of iron, chromium and nickel at pH 10.6 [3]. Only key results are presented and discussed here. The multiple cycles of voltammograms obtained using two different upper scan limits of 0.0 V_{SCE} and 0.7 V_{SCE} are compared in Fig. 1a. The 5th CV cycles obtained with different upper scan limits are compared in Fig. 1b.

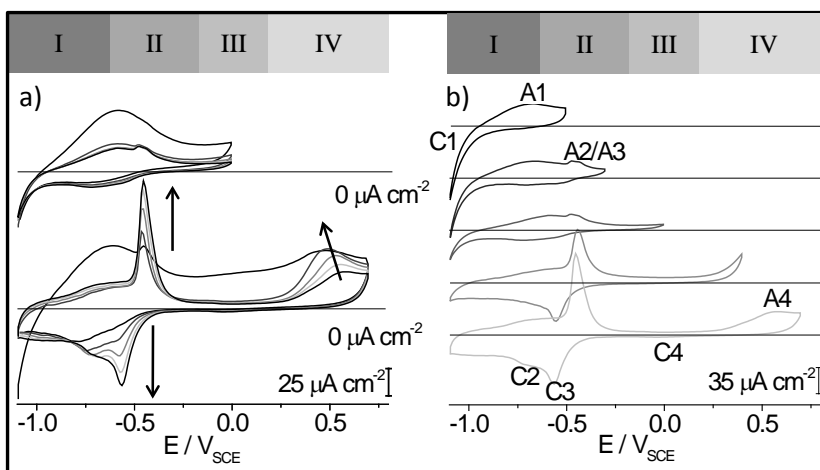


Figure 1. a) Cyclic voltammogram obtained as a function of the number of cycles (1-5) with two different upper scan limits, and b) the fifth cycle of a cyclic voltammogram as a function of the upper scan limit. Horizontal lines in the individual CVs indicate zero measured current. Arrows indicated change in current with increasing scan cycle.

Peak A1: In the potential range of peak A1, the anodic oxidation of Fe to form an Fe^{II} oxide (e.g., FeO/Fe(OH)₂ and FeCr₂O₄) or an Fe^{II/III} oxide (e.g., Fe₃O₄) are thermodynamically possible. Due to the pre-existing chromium oxide layer, the oxides formed in this potential range are likely to be composed of a chromite-like (Fe^{II}Cr^{III}₂O₄) oxide in the inner layer and a magnetite-like (a mixed Fe^{II/III} oxide like Fe₃O₄) oxide in the outer layer.

Peaks A2/A3: A peak A2/A3 appeared when the upper scan limit was greater than 0.0 V_{SCE} . This peak was partially resolved in the 5th cyclic voltammogram into two peaks, hence, the labelling as the peak as A2 and A3 (Fig. 1a). These current peaks were also observed in CVs of carbon steel under the same conditions [4] and were attributed to the conversion of magnetite to γ -Fe₂O₃ (maghemite) phase. The oxidation of hydrated Fe^{II} species to γ -FeOOH is also thermodynamically possible in this range. CVs performed at pH values 11.6 and 12.6 (results not shown) indicate that the oxidation of Fe^{II} to γ -FeOOH becomes significant at pH values higher than 10.6, and occurs at a potential lower than that of peak A2. This process was negligible during CV scans at pH 10.6, however, this oxidation may be able to compete with the oxidation of Fe^{II} to magnetite under potentiostatic conditions (see further discussion in section 3.2).

Peak A4: When the upper scan limit was greater than 0.2 V_{SCE} , a broad anodic peak, A4 appeared. At potentials $> 0.2 V_{SCE}$, the oxidation of magnetite to γ -FeOOH and the oxidation of Cr^{III} to Cr^{VI} are thermodynamically possible. The conversion of magnetite/maghemite to γ -FeOOH on carbon steel is known to lead to film fractures that can be quickly repassivated [4]. This oxidation on SS may expose the inner Cr^{III} layer on the stainless steel surface to the solution and thereby facilitate the oxidation of the Cr^{III} oxide to a highly soluble Cr^{VI} oxide.

Oxidation Potential Regions

From the CV data, four potential regions were identified for anodic oxidation of Type 316L SS at pH 10.6 as indicated in Fig. 1. These were further investigated by potentiostatic measurements and are summarised after the potentiostatic results.

3.2. Oxide Formation and Conversion under Potentiostatic Conditions

Iron and chromium XPS results were deconvoluted using composite reference spectra for oxidised metal species reported elsewhere [5]. In the region $E \leq -0.5 V_{SCE}$, the atomic ratio of total Fe to total Cr increased with increasing E_{APP} . With this decrease is an increase in the ratio of oxide Fe (sum of Fe^{II} and Fe^{III}) to total Fe. These results are consistent with the CV data. In the region $-0.5 V_{SCE} < E < 0.0 V_{SCE}$, the composition ratios of different oxidation states show the opposite trends consistent with the proposed mechanism of forming a passivating Fe^{III} layer.

There is a sharp transition in the potential dependence of the composition of oxide layer at $-0.1 V_{SCE}$, between the regions II and III. This is the equilibrium potential for the magnetite/ γ -FeOOH oxidation. This oxidation can lead to fracture of the passive maghemite layer which promotes the oxidation of Fe and Fe^{II} to magnetite and then to maghemite in the underlying oxide layer, establishing a cycle of film fracture and repair. At $-0.1 V_{SCE}$, the rate of magnetite oxidation to γ -FeOOH is very slow. As the potential increases into region III ($0.0 V_{SCE} < E < 0.2 V_{SCE}$), the oxidation rate of magnetite to γ -FeOOH increases with increasing potential leading to fast film growth via continuous film fracture and repair mechanisms. Consistent with these mechanisms, the XPS results from Ox III show a decrease in the ratio of total Fe to total Cr and an increase in the relative amount of Fe^{III}. In the Ox IV region ($0.2 V_{SCE} < E$), the ratios of Cr^{III} to total Cr and of the oxide Fe (Fe^{II} + Fe^{III}) to total Fe increase, suggesting that chromium dissolution and build-

up of the iron oxide layer are becoming more important.

The oxide formation and conversion kinetics during film growth were investigated by potentiostatic film growth (Fig. 2). In region I, the current quickly reached a near steady state value (Fig. 2a). The constant anodic current can be attributed to the less impeded injection of Fe^{II} into the thin and defective air-formed chromium oxide layer that was initially present on the SS. After this time, the current decreased and eventually switched from anodic to cathodic. This is attributed to the chromite-like layer becoming saturated with Fe^{II} and Fe^{II} transport through the oxide layer slowing down. When this anodic current is sufficiently low, the net current is dominated by the current from the water reduction process.

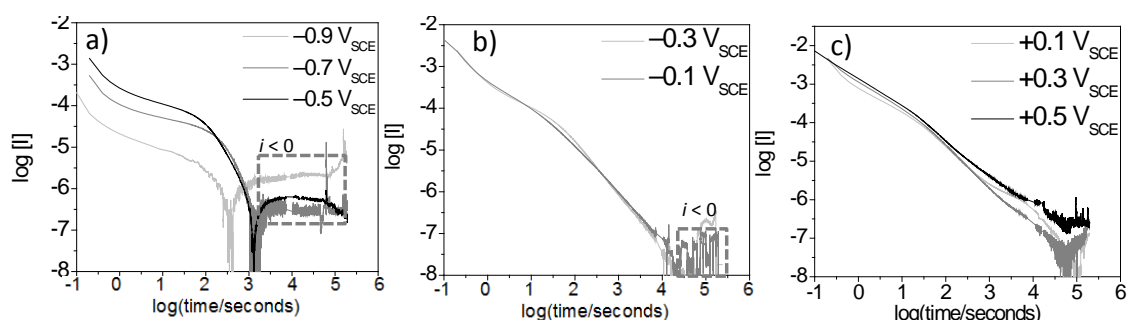


Figure 2. Current as a function of time observed during potentiostatic film growth.

In region II, the slope of $\log i$ vs $\log t$ quickly approached a value of -1 (Fig. 2b). The linear rate suggests uniform oxide layer growth. The time-dependent behaviour of the current in the first 10^3 s (or about 15 min) is nearly independent of the film growth potential in region II and III. This is consistent with the formation of a chromite-like inner oxide layer through which Fe^{II} that is injected at the metal/oxide interface must be transported to the oxide/water interface for further oxidation. In the Ox III region, the oxidative dissolution of chromium results in the small steady-state anodic current that is seen at long intervals ($>10^4$ s).

The surface analyses and electrochemical measurements made for film growth under potentiostatic conditions are consistent with the CV results. Thus, the type of the oxide layer formed and the metal dissolution behaviour for SS during steady-state corrosion under potentiostatic conditions can be summarised as follows. In Ox region I ($E < -0.5 V_{SCE}$), the pre-existing chromium oxide is converted to a chromite-like oxide. As the inner oxide layer is saturated with Fe^{II}, magnetite can form at the outer layer. Once a coherent layer of these oxides is formed, metal dissolution will occur from chromite and magnetite surfaces. Ox region II ($-0.5 V_{SCE} < E < 0.0 V_{SCE}$) consists of the conversion of the pre-existing chromium oxide to a chromite/magnetite-like oxide. This conversion is quickly followed by oxidation of the magnetite to maghemite and the oxidation of hydrated Fe^{II} species to γ -FeOOH. This will form a thin but protective oxide layer. Metal dissolution is limited to surface hydrated Fe^{III} oxides/oxyhydroxides and will be slow. In Ox region III ($0.0 V_{SCE} < E < 0.2 V_{SCE}$), a layer of magnetite/maghemite/ γ -FeOOH on chromite grows rapidly via continuous film fracture and repassivation, resulting in a

porous and less protective layer. The metal dissolution rate will be higher in this region than in the Ox II region. Ox Region IV ($0.2 V_{SCE} < E$) involves dissolution of chromium accompanying the growth of magnetite/ maghemite/ γ -FeOOH in the oxide layer.

4. Conclusion

This study identified four potential regions for oxide formation on Type-316L stainless steel. The region Ox I is for potentials below $-0.5 V_{SCE}$. In this region, the conversion of a pre-existing, but defective, Cr_2O_3 film to a chromite film and growth of an outer magnetite layer can occur. The region Ox II is in the potential range from $-0.5 V_{SCE}$ to $0.0 V_{SCE}$. In this region, additional oxidations of the magnetite to γ - Fe_2O_3 and hydrated Fe^{II} species to γ -FeOOH can occur. The competing reactions for the oxidation of Fe^{II} to magnetite (and to γ - Fe_2O_3) and to γ -FeOOH will affect the nature of the film and dissolution rate. Regions Ox III and Ox IV have potentials $> 0.0 V_{SCE}$. In these regions, the conversion of the maghemite-covered magnetite to γ -FeOOH occurs. The oxide layer grows via film fracture and repair, thus compromising its passivity. A distinction between Ox III and Ox IV arises at $0.2 V_{SCE}$. This is the potential at which oxidative chromium dissolution can occur due to the exposure of the inner chromite layer to the solution.

5. Acknowledgements

This research was funded under the National Science and Engineering Council of Canada and Atomic Energy of Canada Limited Industrial Research Chair Agreement. The electrochemical analysis equipment was purchased with a grant from the Canada Foundation for Innovation.

6. References

- [1] P.A. Yakabuskie, J.M. Joseph, J. Clara Wren, "The effect of interfacial mass transfer on steady-state water radiolysis", *Radiat. Phys. Chem.*, Vol. 79, Iss. 7, pp. 777-785.
- [2] Q.W. Knapp, K. Daub, A.Y. Musa, J.C. Wren, "Comparative study of oxide growth and conversion on stainless steel and carbon steel" In Prep.
- [3] B. Beverskog, I. Puigdomenech, "Revised pourbaix diagrams for nickel at 25-300 °C", *Corrosion Science*, Vol. 39, Iss. 5, 1997, pp. 969-980.
B. Beverskog, I. Puigdomenech, "Revised pourbaix diagrams for iron at 25-300 °C", *Corros. Sci.*, Vol. 38, Iss. 12, 1996, pp. 2121-2135.
B. Beverskog, I. Puigdomenech, "Revised pourbaix diagrams for chromium at 25-300 °C", *Corros. Sci.*, Vol. 39, Iss. 1, 1997, pp. 43-57.
B. Beverskog, I. Puigdomenech, "Pourbaix diagrams for the ternary system of iron-chromium-nickel", *Corrosion*, Vol. 55, Iss. 11, 1999, pp. 1077-1087.
- [4] W. Xu, K. Daub, X. Zhang, J.J. Noel, D.W. Shoesmith, J.C. Wren, "Oxide formation and conversion on carbon steel in mildly basic solutions", *Electrochim. Acta*, Vol. 54, Iss. 24, 2009, pp. 5727-5738.
- [5] M.C. Biesinger, B.P. Payne, A.P. Grosvenor, L.W.M. Lau, A.R. Gerson, R.S.C. Smart, "Resolving surface chemical states in xps analysis of first row transition metals, oxides and hydroxides: Cr, mn, fe, co and ni", *Appl. Surf. Sci.*, Vol. 257, Iss. 7, 2011, pp. 2717-2730.